AD-A060 084 NAVAL ACADEMY ANNAPOLIS MD MICHELSON PHYSICAL LAB F/G 20/4
ACOUSTIC CAVITATION INCEPTION IN WATER AND IN INSONATED ROOT TI--ETC(U)
SEP 78 L A CRUM

UNCLASSIFIED TR-178 NL

1 OF 1
AD
A0 60084

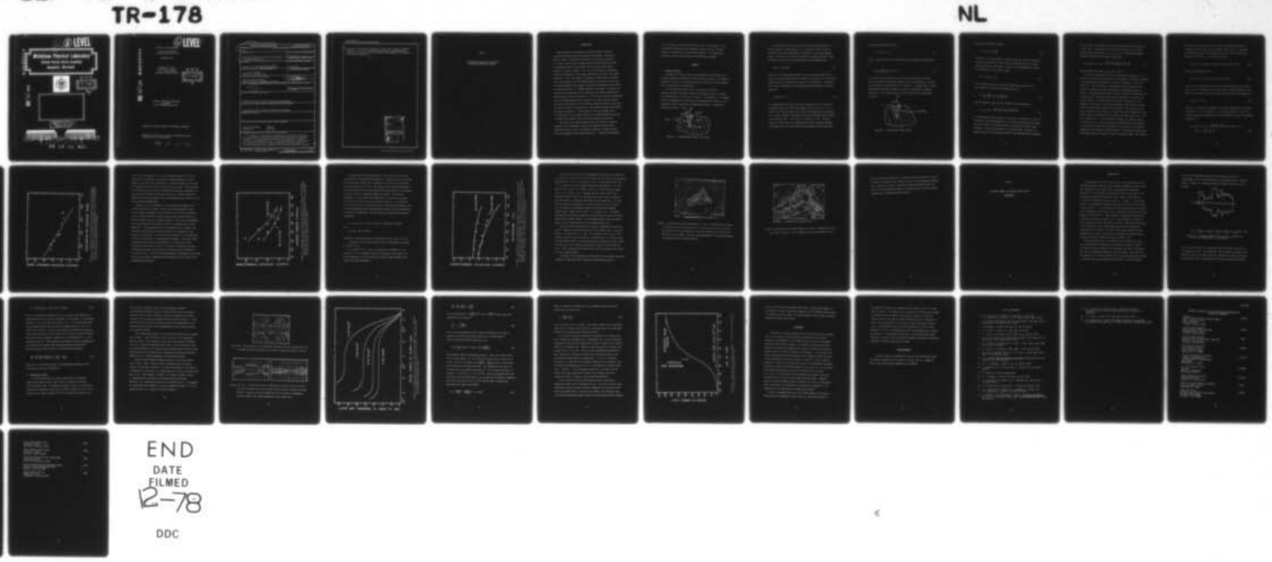

END
DATE
FILMED
12-78
DDC

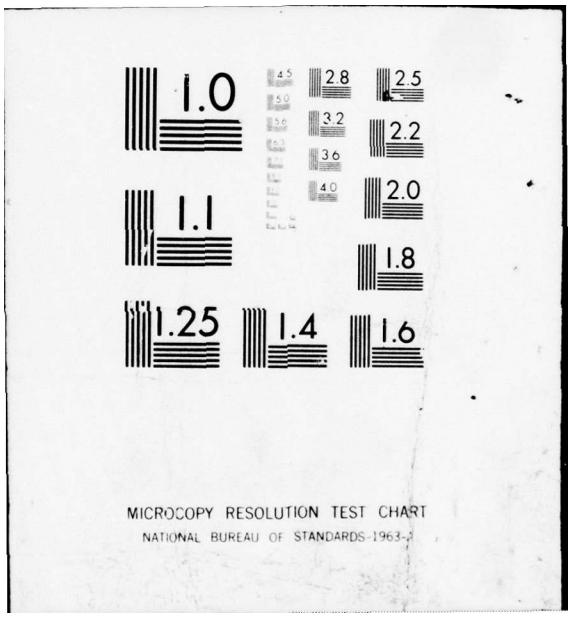
1.0
1.1
1.25
1.4
1.6
1.8
2.0
2.2
2.5
2.8
3.2
3.6
4.0
4.5
5.0
5.6
6.3
MICROCOPY RESOLUTION TEST CHART
NATIONAL BUREAU OF STANDARDS-1963-A

(12) (8) LEVEL II

AD A060084

Michelson Physical Laboratory

United States Naval Academy

Annapolis, Maryland

(6) LEVEL II

OFFICE OF NAVAL RESEARCH

Contract NR 384-923
Technical Report No. 178

September 1978

Lawrence A. Crum
Department of Physics
U. S. Naval Academy
Annapolis, Maryland 21402

ACOUSTIC CAVITATION INCEPTION IN WATER AND IN INSONATED ROOT TIPS

UNCLASSIFIED

SECURITY CLASSIFICATION OF THIS PAGE *(When Data Entered)*

REPORT DOCUMENTATION PAGE	READ INSTRUCTIONS BEFORE COMPLETING FORM
1. REPORT NUMBER: TR-178	2. GOVT ACCESSION NO.
3. RECIPIENT'S CATALOG NUMBER	
4. TITLE *(and Subtitle)*: ACOUSTIC CAVITATION INCEPTION IN WATER AND IN INSONATED ROOT TIPS.	5. TYPE OF REPORT & PERIOD COVERED: TECHNICAL / Interim
6. PERFORMING ORG. REPORT NUMBER	
7. AUTHOR(s): ASSOCIATE PROFESSOR LAWRENCE A. CRUM	8. CONTRACT OR GRANT NUMBER(s): NR 384-923
9. PERFORMING ORGANIZATION NAME AND ADDRESS: U. S. NAVAL ACADEMY, ANNAPOLIS, MARYLAND 21402	10. PROGRAM ELEMENT, PROJECT, TASK AREA & WORK UNIT NUMBERS
11. CONTROLLING OFFICE NAME AND ADDRESS: OFFICE OF NAVAL RESEARCH, 800 N. QUINCY ST., ARLINGTON, VA 22217	12. REPORT DATE: 15 SEPTEMBER 1978
	13. NUMBER OF PAGES: 41
14. MONITORING AGENCY NAME & ADDRESS *(if different from Controlling Office)*: 43 p.	15. SECURITY CLASS. *(of this report)*: U
	15a. DECLASSIFICATION/DOWNGRADING SCHEDULE

16. DISTRIBUTION STATEMENT *(of this Report)*

APPROVED FOR PUBLIC RELEASE: DISTRIBUTION UNLIMITED

17. DISTRIBUTION STATEMENT *(of the abstract entered in Block 20, if different from Report)*

APPROVED FOR PUBLIC RELEASE; DISTRIBUTION UNLIMITED

18. SUPPLEMENTARY NOTES

19. KEY WORDS *(Continue on reverse side if necessary and identify by block number)*

ACOUSTIC CAVITATION
NUCLEATION
BUBBLES
ROOT TIPS

20. ABSTRACT *(Continue on reverse side if necessary and identify by block number)*

An analysis of two aspects of air bubble nucleation is presented. Part I describes the role of particulate matter in acoustic cavitation inception; Part II describes the growth of air bubbles by rectified diffusion in insonated root tips. It was discovered that a modification of some earlier analyses of cavity nucleation from motes leads to a correct prediction of the variation of the acoustic cavitation inception → next page

DD FORM 1 JAN 73 1473 EDITION OF 1 NOV 65 IS OBSOLETE S/N 0102-014-6601 | 405 634

UNCLASSIFIED

SECURITY CLASSIFICATION OF THIS PAGE *(When Data Entered)*

cont. threshold for kilohertz frequencies in water for a range of physical variables. It was also discovered that acoustic emissions from insonated root tips could be attributed to the growth of air bubbles by rectified diffusion.

PART I

A QUANTITATIVE ANALYSIS OF ACOUSTIC CAVITATION INCEPTION IN WATER

INTRODUCTION

Many attempts have been made to explain acoustic cavitation inception thresholds but have achieved little success. The work of Harvey,[1] Barger,[2] Strasberg,[3] and Apfel[4] is well known, and Holl,[5] in a recent review, lists 51 papers concerning the inception problem. A historical survey of the problem will not be given here; recent reviews[5,6] are quite complete. The crux of the problem in explaining cavitation thresholds is the proper treatment of the nuclei that induce cavitation. Holl,[5] for example, concludes his review with the comment "It is very apparent that the understanding of the onset of cavitation is greatly dependent upon knowing the form, size distribution and source of cavitation nuclei." A renewed interest in the onset of cavitation in liquids has been generated by the discovery that polymer additives that reduce drag also reduce cavitation.[7,8] This point is now well established and is of considerable interest because of its double positive effect. An adequate explanation of the cavitation reduction problem has not been given but attention is being given to fluid dynamics rather than effects of physical parameters. In particular, Ellis[9] has commented that "an explanation of the reduced cavitation in polymer solutions must lie in changed flow dynamics rather than fluid physical properties".

This report will present evidence that the cavitation inception threshold can be explained in terms of nucleation from gas-filled cavities in motes, that is, microscopic particles of nonpolar solids that are suspended in the cavitating liquid. A theoretical expression

for the cavitation threshold will be given that is independent of the geometrical properties of the suspended particle and that correctly predicts the behavior of the cavitation threshold with temperature, frequency, liquid surface tension and dissolved gas content.

RESULTS

A. Theoretical model

The model that will be used is one originally due to Harvey[1] that has been modified by Strasberg[3] and more recently by Apfel.[4] The general approach of Apfel will be followed; however, details of the calculations will be given here for completeness.

It is assumed that there exist in the body of the fluid numerous particles of nonpolar solids that contain gas that is trapped in irregularities in the particle's surface. For simplicity it is assumed that the irregularities containing the entrained gas are cones, but the approach is easily generalized to wedge-shaped cracks. A model mote is drawn in the Fig. 1 below.

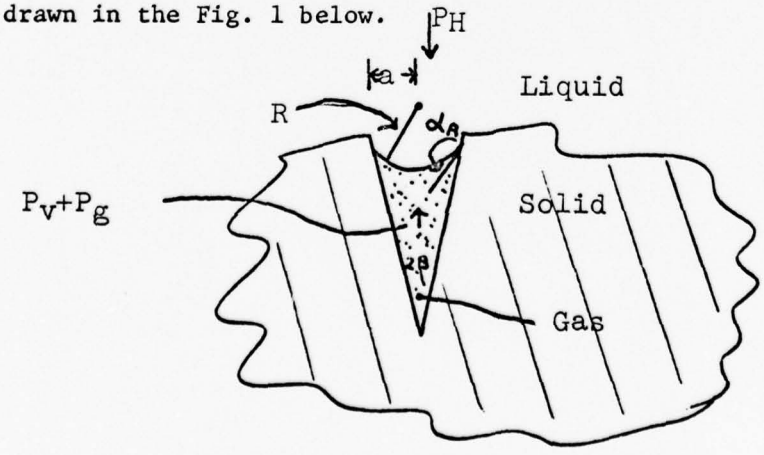

Figure 1. Mathematical model of a mote.

In order for this mote to be an effective cavitation nucleus, it must be capable of stabilization, i.e., it must not allow the gas to dissolve in the normal experimental condition of a partially degassed liquid. This will occur when the interface is concave outwards to such an extent that forces on the interface are in equilibrium, viz.,

$$P_H = P_v + P_g + \frac{2\sigma}{R} , \tag{1}$$

where P_H is the hydrostatic pressure, P_v is the vapor pressure of the liquid, P_g is the equilibrium gas content of the liquid, σ is the surface tension and R is the radius of curvature of the interface. In addition there exist requirements on the advancing contact angle α_A and crevice angle 2β;

$$\beta + \frac{\pi}{2} \leq \alpha_A \leq \pi . \tag{2}$$

It is appropriate now also to make the assumption that for crevices to be effective they must have small angles, that is, $\cos \beta \approx 1$. It is known[10] that nonpolar solids that are good candidates for mote material, e.g., parafin, beeswax, cellulose acetate have advancing contact angles on the order of 100°. Thus, for Eq. 2 to hold, $\beta \approx 10°$. If motes similar to these exist in a degassed liquid, the air-liquid interface will advance until the above equations are obeyed, and will then stop.

At this stabilization position,

$$a = R \cos (\alpha_A - \beta) \ . \tag{3}$$

If Eq. 1 is solved for R, the half-width of the crevice can be expressed as

$$a = \frac{2\sigma}{P_H - P_v - P_g} \cos (\alpha_A - \beta) \ . \tag{4}$$

If we assume that the motes are all nonpolar solids such as parafin, and the crevices all have small angles, then it is convenient to set the contact angle relationship equal to a constant δ. Consider next a typical experimental situation in which the liquid is subjected to a negative pressure P_L. The interface will now bow out and take the shape shown in Fig. 2.

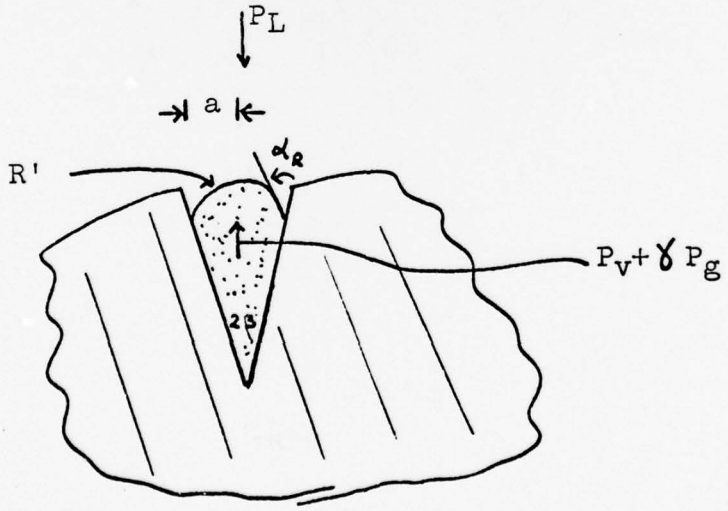

Figure 2. Nucleation from a mote.

The force balance now requires

$$P_L = P_v + \gamma P_g - \frac{2\sigma}{R'} . \tag{5}$$

The factor γ has been added to account for the fact that in the dynamic situation the diffusion of gas across the interface may not be rapid enough to maintain equilibrium. Again, R' can be expressed in terms of the liquid-solid contact angle, α_R as

$$R' = a/\cos (\alpha_R - \beta) . \tag{6}$$

a has already been set by the initial conditions as given in Eq. 4. The radius of curvature of the interface is then

$$R' = \frac{2\sigma}{P_H - P_v - P_g} \frac{\delta}{\cos (\alpha_R - \beta)} , \tag{7}$$

and the pressure balance on the interface can be expressed as

$$P_L = P_v + \gamma P_g - \frac{(P_H - P_v - P_g)}{\delta} \cos (\alpha_R - \beta) . \tag{8}$$

If the negative pressure imposed on the liquid is sufficient to cause the interface to become hemispherical or to reach the receding contact angle, then the interface will advance along the crevice and is said to have nucleated. Since we have assumed β to be quite small, and since it is known that $\alpha_R \approx 40°$ for nonpolar solids,[10] the requirement for nucleation

will be taken as the condition that the interface achieve the receding contact angle. The pressure in the liquid is related to the acoustic pressure by the relation $P_A = P_L - P_H$, so that the acoustic pressure amplitude required for cavitation inception is

$$P_A = -(P_H - P_v - \gamma P_g) - \frac{(P_H - P_v - P_g) \cos(\alpha_R - \beta)}{\delta} . \qquad (9)$$

This is essentially equal to Eq. 3-13a of Ref. 4.

In order to apply this theory to an experimental situation, it is necessary to specify the contact angle relationships. The actual procedure of the experimental measurements is also very important. To test the theory, Eq. 9 will be applied to measurements of the variation of the cavitation threshold with gas concentration, temperature, and surface tension. The variation with surface tension is particularly important for it requires that the contact angles also be expressed as a function of surface tension. In the experimental procedure, the liquid is first degassed to a particular value, varying amounts of surfactant are added, and then the cavitation threshold is determined. The initial position of the interface in the crevice is set when the surface tension is at its initial value, and when surfactant is added, does not change; thus, δ is not a function of σ. As the surfactant is added, the surface tension is reduced, but Eq. 1, which specifies the conditions for the equilibium of the interface, shows that the radius of curvature will then reduce to compensate for the change in surface tension. The receding contact angle relationship will be a function of surface tension, however. For nonpolar

solids such as parafin there is a significant hysteresis between the equilibium contact angle and the receding contact angle.[11] Hysteresis is necessary for this stabilization mechanism to work, of course, and must be accounted for. It is possible to write

$$\cos(\alpha_R - \beta) = \cos(\alpha_e - \alpha_H - \beta) = \cos[\alpha_e - (\alpha_H + \beta)] , \tag{10}$$

which can be expanded to give

$$\cos(\alpha_R - \beta) = \cos\alpha_e \cos(\phi) + \sin\alpha_e \sin(\phi) , \tag{11}$$

where α_e is the equilibium contact angle, α_H is the amount of hysteresis and $\phi = \alpha_H + \beta$. Bargeman and Van Voorst Vader[12] have determined that the effect of surfactants on the equilibium contact angle can be expressed by

$$\cos\alpha_e = -1 + C/\sigma , \tag{12}$$

where C is a constant that depends on the surface properties of the solid. For parafin, C = 49, for beeswax, C = 48; we have chosen C = 48.5. The acoustic cavitation threshold can then be expressed in terms of measureable parameters as

$$P_A = (P_H - P_v - \gamma P_g) - \frac{(P_H - P_v - P_g)}{\delta}\left[\cos(\phi)(C/\sigma - 1) + \sin\phi\left[1 - \left(\frac{C}{\sigma} - 1\right)^2\right]^{1/2}\right] \tag{13}$$

B. Application of theory to experimental results

The incipient threshold was measured for acoustic cavitation in distilled water. Various hollow piezoelectric cylindrical transducers were used that were open at one end and closed at the other with a tightly stretched stainless steel foil. A typical one would have an inside diameter of 6.2 cm, a height of 7.5 cm and would be driven in $(r,\theta,z) = (3,0,3)$ normal mode. Higher modes restricted the cavitation to a localized area in the interior of the cylinder of liquid, away from walls and boundaries. Most measurements were made at a frequency of 36 kHz. The threshold was determined by increasing the acoustic pressure amplitude a small amount, waiting for a fixed time (normally one minute), increasing the amplitude and so forth until an audible snap was heard. The pressure amplitude was then decreased to zero for a few minutes, and the measurement repeated several times. Fresh samples were allowed to "age" before measurement and data that had a time dependence were discarded. Measurements of the physical parameters such as surface tension, gas content and temperature were measured in situ by a du Nuoy ring tensiometer, an oxygen electrode and a bead thermister, respectively. The acoustic pressure amplitude was measured at the center of the cavitation zone by a calibrated hydrophone as a function of input current to the transducer and the cavitation chamber calibrated in terms of this input current.

In order to test the theory, measurements were made of the variation of the incipient cavitation threshold as a function of dissolved gas content, temperature, and surface tension. These data are shown in

Figs. 3, 4 and 5, respectively. Equation 13 contains three constants that can not be specified initially. These constants are: γ, a constant that measures the ability or inability of diffusion to keep pace with the rapidly expanding cavity; δ, a measure of the advancing contact angle; and ϕ, a measure of the hysteresis between the advancing and receding contact angles. Equation 13 was then applied to the data in Figs. 3, 4 and 5 and a best fit obtained. The values of the constants obtained were $\gamma = 1.0$, $\delta = 0.038$ and $\phi = 35°$. The implications of these constants will be discussed later.

As a further result, ordinary tap water was filtered with a Millipore filter with a pore size of 0.45μ and the particulate matter examined with a scanning electron microscope. Figures 6 and 7 show photomicrographs of the particulate matter examined. Note the tremendous number of sites that are available for gas entrainment--one particle such as this could provide nuclei for thousands of cavitation events. It is also to be noted that the crevices are small angled, in support of our initial hypothesis of $\cos \beta \approx 1$.

DISCUSSION

We have produced a theoretical prediction of the incipient threshold for acoustic cavitation inception and have compared our predictions with experimental measurements. In Fig. 3 it is seen that good agreement is obtained between theory and experiment for the variation of the cavitation threshold with dissolved gas content. We have found

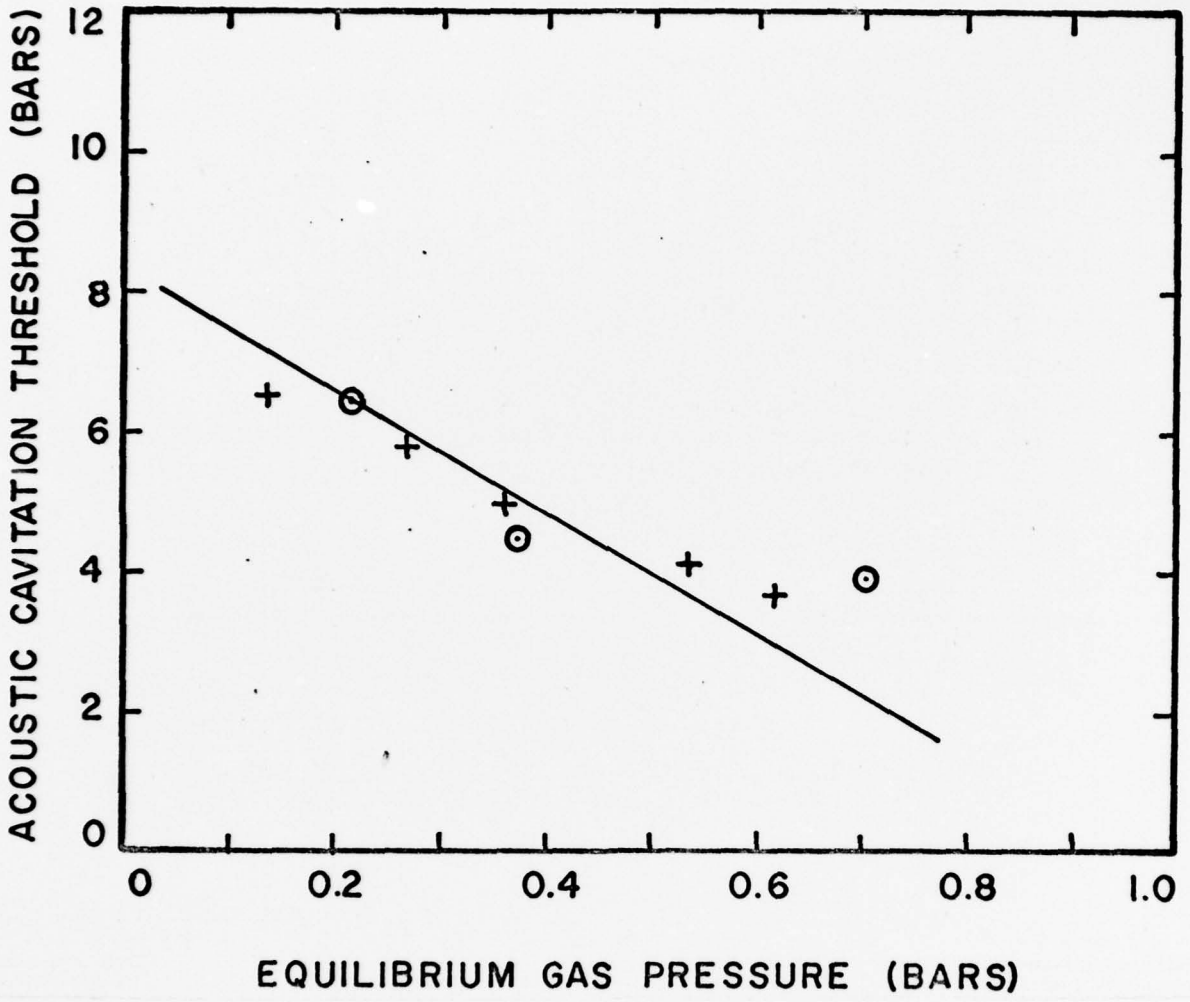

Figure 3. Variation of the cavitation threshold with dissolved gas content. The curve is for Eq. 13 with γ =1.0, δ =0.038 and ϕ=35°. The plus signs are experimental measurements from this study; the circles are values obtained by Strasberg.

that a best fit required $\gamma = 1.0$; an interesting result in that this indicates that diffusion of gas into the expanding nucleus is rapid enough to keep pace with the expansion. Perhaps it should be said that the expansion is slow enough for diffusion to keep pace. This agreement is a welcome result for several observers have noted the dependence of the cavitation threshold on the gas content but a correct theoretical prediction of both the magnitude and the dependence of the effect has not been previously demonstrated.

Figure 4 shows the dependence of the cavitation threshold on the surface tension of the liquid. Most cavitation researchers[13] would expect a direct dependence of the threshold on the surface tension due to the oft-used term $2\sigma/R$ to measure the pressure in the interior of a cavity of radius R due to a surface tension σ. Hoyt[8] has even suggested that one would expect the analysis of Apfel[4] to predict such a direct dependence. The experimental result is promising for it suggests that cavitation reduction may result from addition of surfactants to the liquid to be cavitated. It is seen that an increase in the threshold by a factor of nearly four is experimentally realizable. The author plans to suggest this effect as an explanation for the reduction in the cavitation index observed by Hoyt,[8] and others, in liquids containing drag-reduction agents, which reduce the surface tension considerably. It is seen in Fig. 4 that the inverse dependence is predicted by the theory as well as the correct magnitude of the threshold for two values of the equilibrium gas pressure.

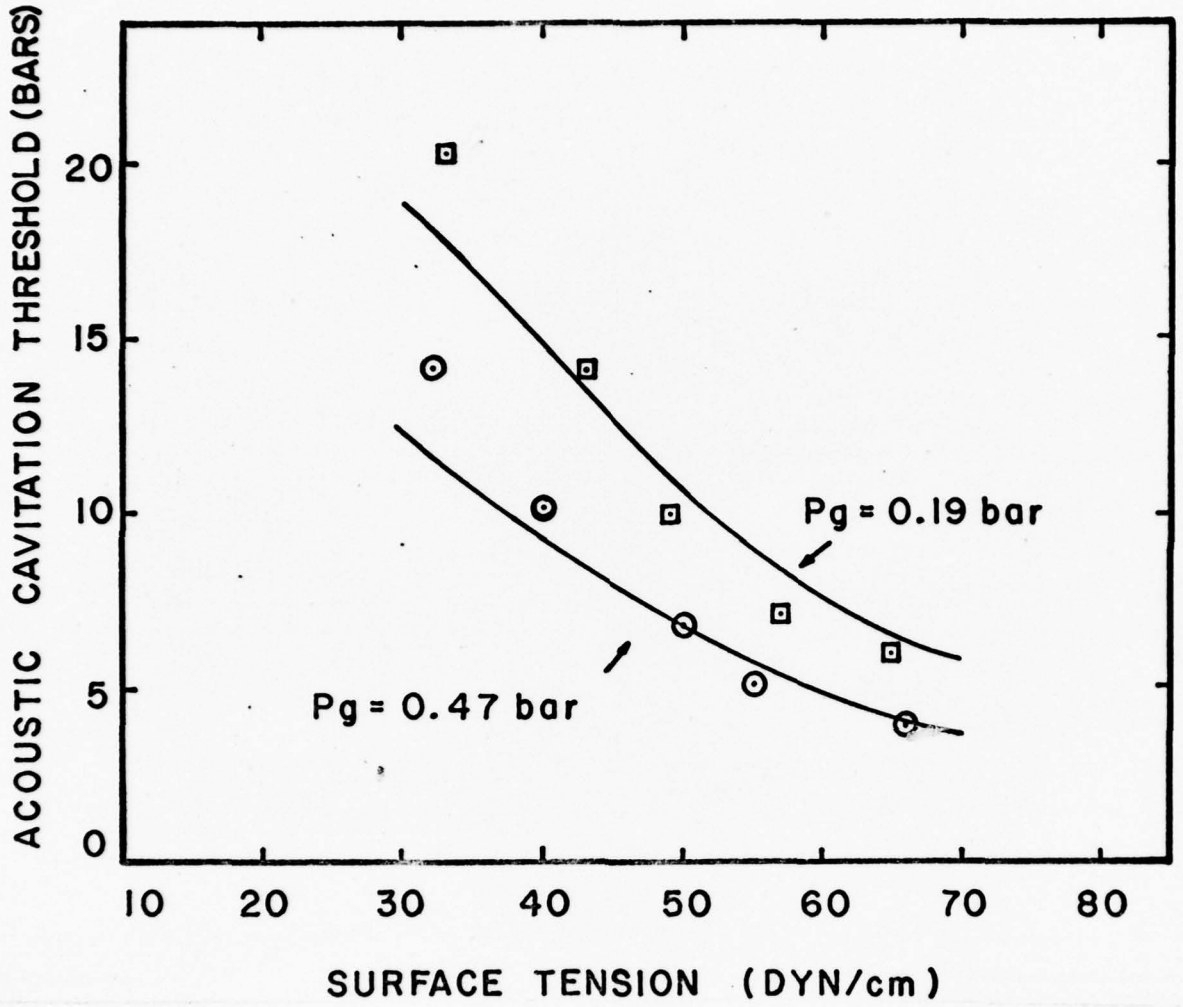

Figure 4. Variation of the cavitation threshold of water with surface tension for two values of the equilibrium gas pressure. The curves are for Eq. 13 with γ =1.0, δ =0.038 and ϕ =35°. The frequency was 36 kHz and the temperature was 25°C.

A further test of the applicability of the theory is its ability to describe the variation with temperature. Figure 5 shows the variation with temperature obtained for a frequency of 22 kHz and an equilibrium gas concentration of 0.35 bar. Also shown are the normalized results of Galloway[14] who had calibration problems and lists values of the threshold at least an order of magnitude higher than others. His measured dependence of the threshold with temperature is seen to be confirmed by the theory as well as our own measured variation. It is important to note that in order to obtain the correct theoretical dependence, both the vapor pressure and the equilibrium gas pressure must be expressed as a function of temperature. We have used the following variations with temperature

$$P_v = (1.61 - (1.03 \times 10^{-1})T + (6.25 \times 10^{-3})T^2) \times 10^4 \quad \text{dyn/cm}^2$$

and

$$P_g = P_g^\circ \quad (0.50 + 0.02T),$$

where P_g° is the equilibrium gas concentration at 25°C and T is in $^\circ$C.

It should be noted that the major effect of temperature is through P_g rather than P_v.

It is noted in Eq. 13 that the threshold is independent of the frequency. For the kilohertz range of frequencies, there seems to be little dependence on the frequency[2] and thus our result predicts the correct frequency dependence.

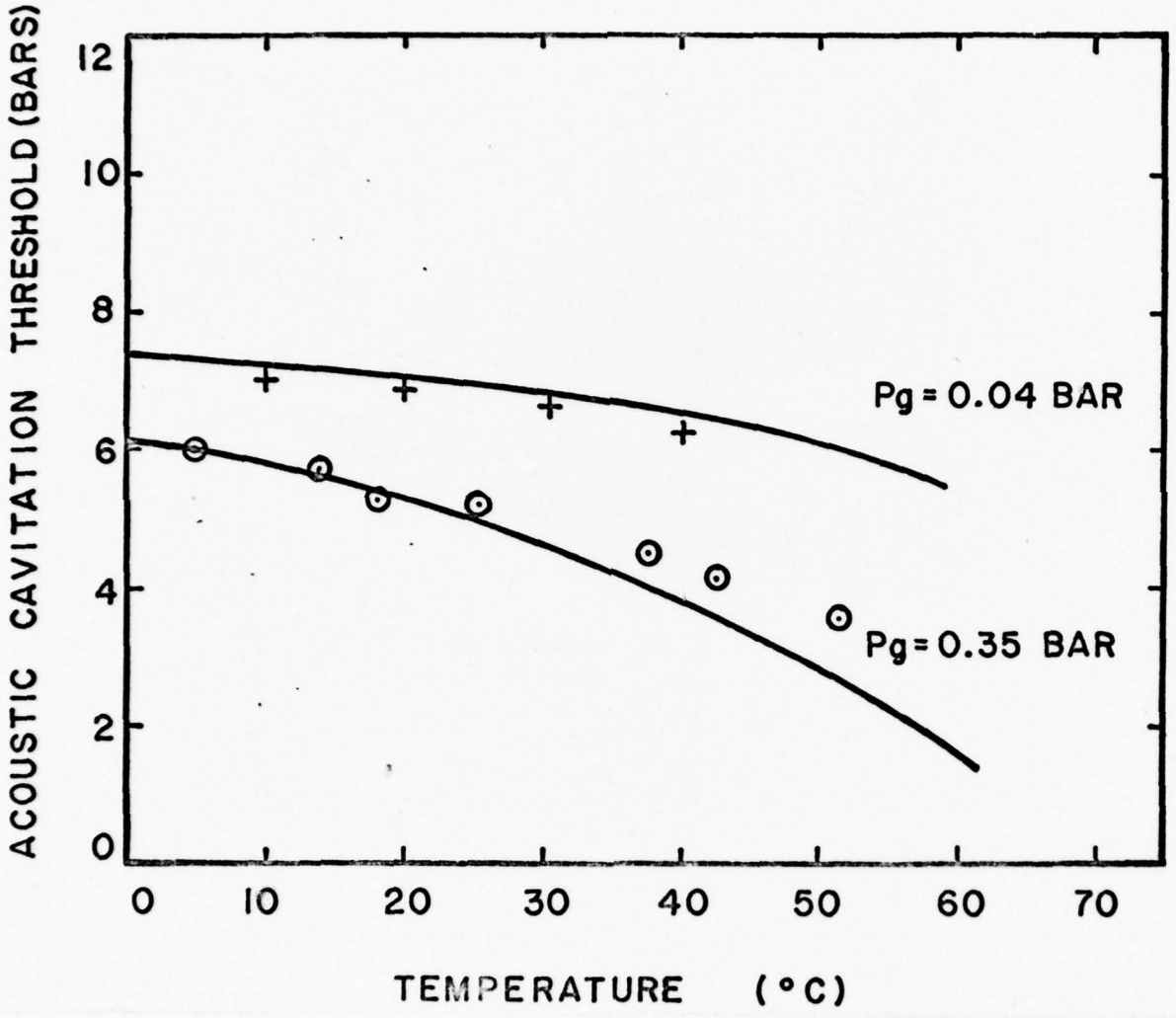

Figure 5. Variation of the cavitation threshold of water with temperature for two values of the equilibrium gas pressure. The curves are for Eq. 13 with $\gamma = 1.0$, $\delta = 0.038$ and $\phi = 35^{\circ}$. The frequency was 22 kHz and the surface tension was 70 dyn/cm. The plus signs are the normalized values of Galloway[14]; the circles are measurements from this study.

In order to obtain the correct magnitudes of the theory to agree with the results of Figs. 3, 4 and 5 it was noted that the value of the constants required were $\gamma = 1.0$, $\delta = 0.038$ and $\phi = 35°$. It was noted earlier that $\gamma = 1.0$ indicated that no diffusion correction was required. $\delta = 0.038$ implies that $\cos(\alpha_A - \beta) = 0.038$. Thus $\alpha_A = \beta + 88°$, and if we assume that $\beta \approx 15°$, then $\alpha_A \approx 103°$. Bargeman and Van Voorst Vader[12] have obtained a value of 106.5° for the advancing contact angle of distilled water on parafin, in excellent agreement with our prediction. The other constant used in the analysis is ϕ which is given by $\phi = \alpha_H + \beta$ where α_H is the degree of hysteresis between the advancing and receding contact angle. Again, if we allow $\beta \approx 15°$, then $\alpha_H \approx 20°$. Furmidge[11] has measured the angle of hysteresis for surfactant plus water on parafin, beeswax and cellulose acetate. His measurements give a mean hysteresis angle of 26.7°, which agrees with our required angle of 20°.

We can use these constants also to obtain an estimate of the size of nuclei. Equation 4 gives the half-width of the crevice mouth. Using the values $\sigma = 70$ dyn/cm, $P_H - P_v - P_g \approx 1 \times 10^6$ dyn/cm^2 and $\cos(\alpha_A - \beta) = 0.038$ we find that the full width of a nucleation site in a crevice would be approximately 0.05μm. The scanning electron micrograph in Fig. 7 shows that the tops of the crevices and cracks on a mote are on the order of 0.5μm. Thus, nucleation sites would arise from air trapped in the bottoms of some of these crevices.

In summary, we have measured the variation of the incipient cavitation threshold in water with such variables as dissolved gas content,

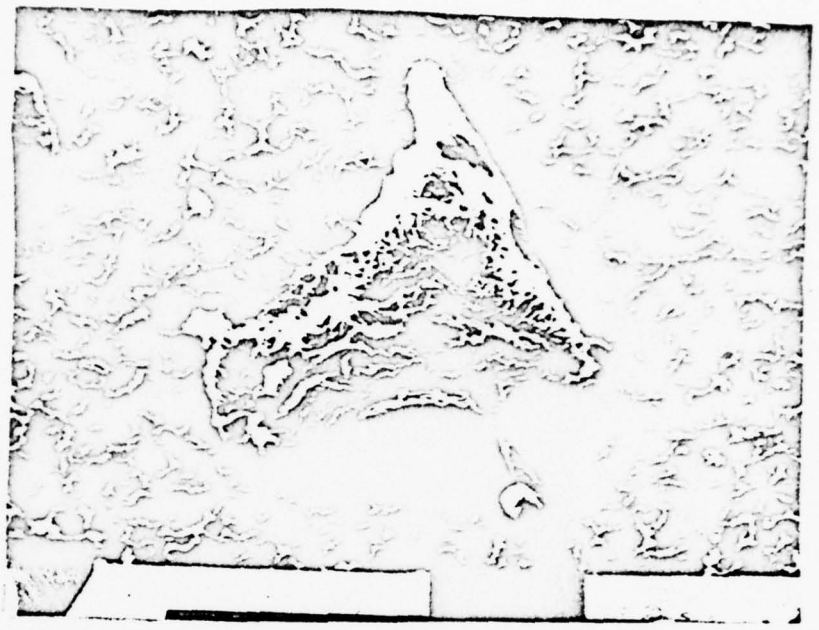

Figure 6. Scanning electron photomicrograph of a mote. The particle was removed by filtration of distilled water with a 0.45 μm pore size filter, shown as the mottled area in the background. The solid horizontal bar in the foreground is a 10 μm marker. Note the ragged appearance of the surface showing the numerous possible nucleation sites.

Figure 7. Scanning electron photomicrograph of a mote. Enlarged view of the mote shown in Figure 6. The horizontal bar in the foreground is 4 μm.

surface tension and temperature. We have modified the analysis of Apfel[4] to obtain an expression that correctly predicts the experimental dependencies. Finally, our model of nucleation from small-angled crevices and cracks in solid particulate matter is substantiated by scanning electron micrographs of filtered particulate matter.

PART II

AIR BUBBLE GROWTH IN INSONATED ROOT TIPS OF *VICIA FABA*

INTRODUCTION

The exposure of the tips of root tips to sound irradiation in the megahertz frequency range can lead to growth retardation or death of the tip, depression of the mitotic index and induction of chromosomal anomalies.[15] The threshold for damage at 1.0 MHz is a function of the ultrasonic intensity and irradiation time[16] and is in the range 0.4 - 0.7 W/cm^2 for irradiation times as long as 2 - 3 hours. If the acoustic intensity is increased to levels on the order of 10 W/cm^2, the root tips often are killed.[17] It is believed that the damage induced by the ultrasonic irradiation is the result of the activation of gas bubbles that are present in the root tip.[18] Large amounts of intercellular gas exist in a growing root system; Gershoy[18] et al., have examined the effects of sound irradiation on the activation of this gas. They have observed that the intercellular gas has caused significant acoustic streaming at intensities on the order of 0.35 W/m^2, with gradual increase until at intensities of 35 W/m^2, free mixing of cytoplasm and vacuolar contents occurred with rapid streaming involving the entire cell.

Since gas bubbles that are activated by sound fields emit white noise, subharmonics and harmonics of the driving frequency, Coakley[19] has examined acoustic emissions from insonated root tips to investigate the role of activated gas bubbles in root-tip damage. His system was very sensitive to acoustic emissions from the root tip during irradiation in that the root tip was placed near the center of a ring transducer.

He found that subharmonic and white noise emissions occurred at approximately the same intensity and had an intriguing history. Figure 8 below is a sketch of a typical subharmonic emission from a root tip at 50 W/cm^2.

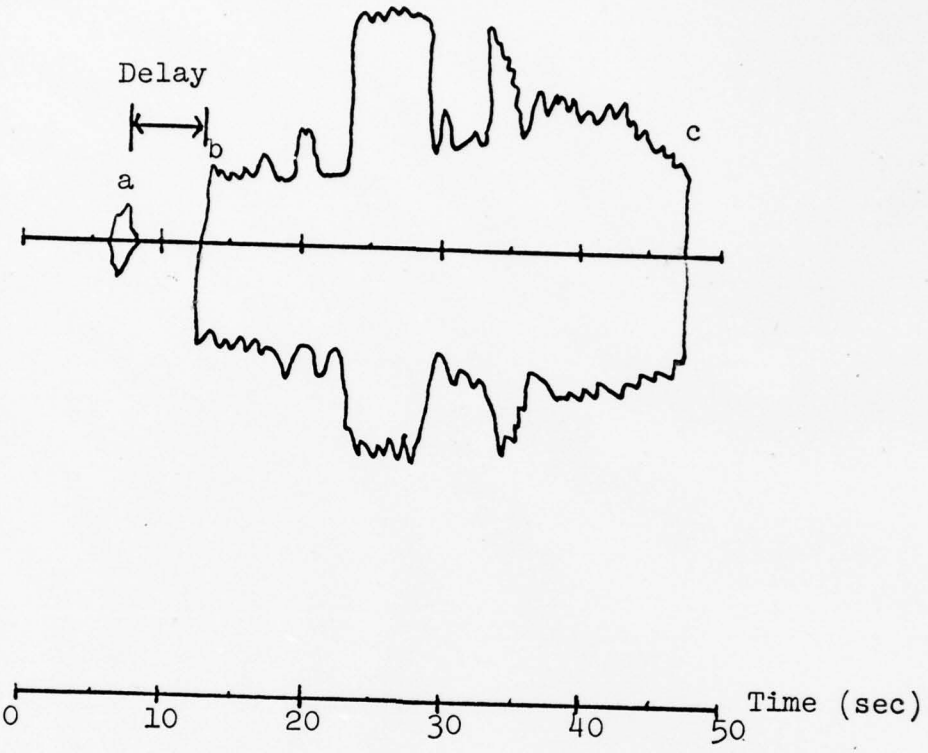

Figure 8. Typical subharmonic envelope. a-sound on, b-onset of subharmonic, c-sound off.

It is noted that there was a significant delay time before the onset of the subharmonic signal. The subharmonic then increased in intensity quite rapidly and grew to a maximum intensity. There was a gradual reduction in intensity until after a few minutes only sporadic activity was observed.

The relatively long delay time between the initial irradiation and the onset of the subharmonic looked very much as if this could be the result of the growth of bubbles by rectified diffusion to near resonance size, where they would pulsate nonlinearly and emit a significant amount of radiation. The variation of the delay time with intensity seemed to confirm this speculation as there was a significant dependence of the delay time on irradiation intensity, as shown in Fig. 9. An attempt was made to explain this delay time in terms of the growth of small nuclei by rectified diffusion.

RESULTS

A. Applicable equations

The equation governing the rate of change of the radius of an air bubble with time is given by Eller[20] to be

$$\frac{dR}{dt} = \frac{Dd}{R}\left(\frac{2(1 - \beta^2/8)}{3(1 - \beta^2)^2}\left(\frac{P_A}{P_0}\right)^2 - \frac{2\sigma}{P_0 R}\right), \tag{14}$$

where D is the diffusion constant, d is the ratio of the concentration, in mass per unit volume, of dissolved gas to the density of the gas in equilibrium with the solution, P_A the acoustic pressure amplitude, P_0 the ambient pressure, and σ the surface tension. The resonance factor β^2 is given by

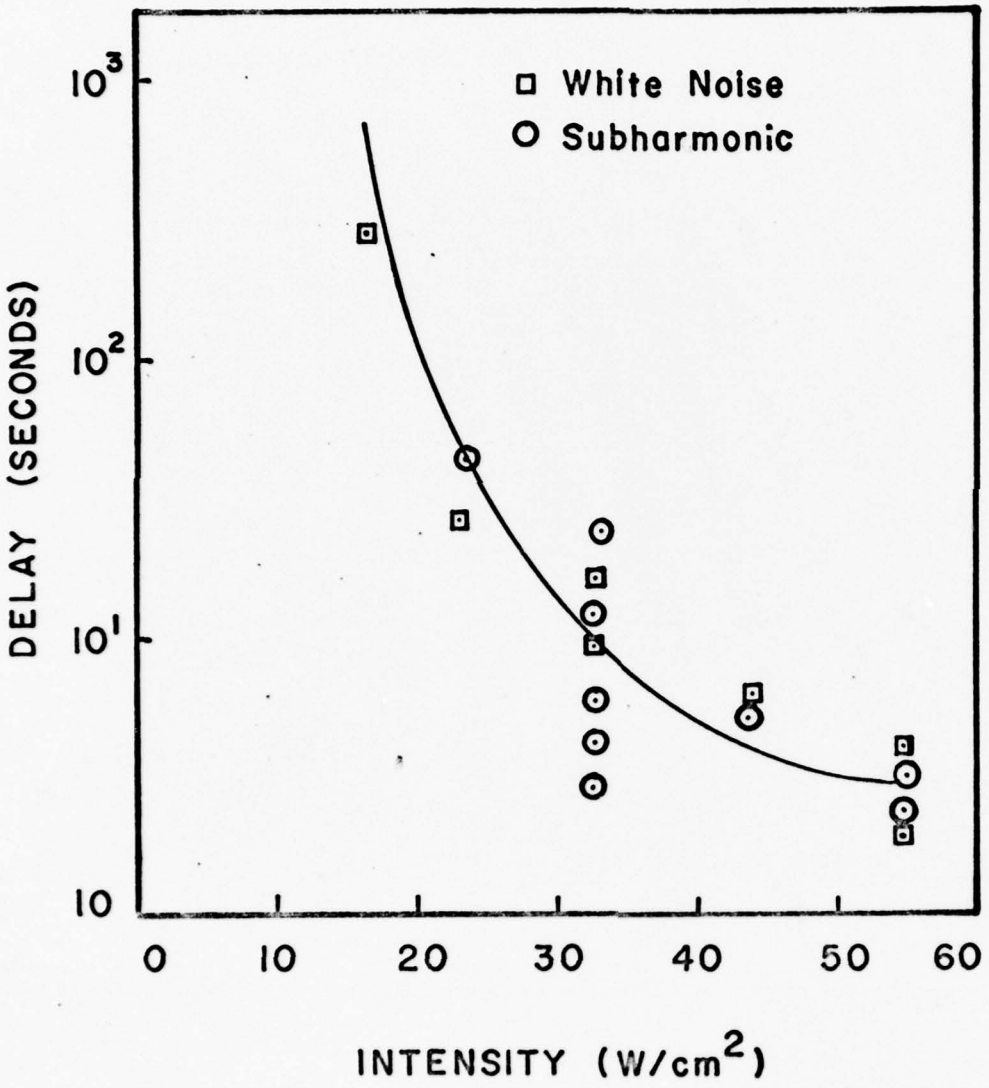

Figure 9. Variation of the delay time for noise emmission with acoustic intensity for irradiated root tips (results of Coakley[19]).

$$\beta^2 = \rho\omega^2 R^2/[3\eta(P_0 - P_v) + (3\eta - 1)2\sigma/R] \ , \qquad (15)$$

where ω is the angular frequency and η is a constant that measures the thermal behavior of the gas in the interior of the bubble. For isothermal behavior, $\eta = 1.0$; for adiabatic cases, $\eta = 1.4$. It was discovered that for air bubbles driven near or below the resonance size at 1 MHz, η is within 2% of being 1.0. Since it was desired to integrate this equation from nuclei-type sizes to the resonance size, it was necessary to account for behavior near resonance. Equation 14 is undefined when $\beta^2 = 1$, the resonance condition. This equation was modified by adding a damping term that prevents the equation from becoming undefined at resonance.[18] Thus, the equation that was used to calculate growth times was

$$\frac{dR}{dt} = \frac{Dd}{R}\left(\frac{2(1 - \beta^2/_8)}{3[(1 - \beta^2)^2 + \xi^2]}\left(\frac{P_A}{P_0}\right)^2 - \frac{2\sigma}{P_0 R}\right) \ , \qquad (16)$$

where ξ^2 is a complicated function of thermodynamic constants and is discussed in more detail elsewhere.[21]

B. Theoretical results

It was discovered that for these large acoustic intensities, bubbles would grow from very small sizes to resonance size within relatively short times. By computer integration of Eq. 16 it was found that the time required to grow from an initial radius of 5×10^{-6} cm to resonance size, which is about 3.2×10^{-4} cm, was on the order of 1 ms

for the lowest intensity found to cause subharmonic emission (approximately 20 W/cm^2). Conditions within the root tip are obviously different from the ideal conditions specified for growth by rectified diffusion but four orders of magnitude seem too much to make up. It was concluded that the delay time observed between the commencement of the irradiation and the onset of the subharmonic was very likely not growth by rectified diffusion.

It was discovered, however, that rectified diffusion effects appeared to be present. Figure 10a shows a fast trace scan of the subharmonic emission output. There appeared in each trace several growth sequences that had relatively consistent growth times. In this particular scan, 10 growth sequences can be observed with an average growth time of 0.3 ms. These times are on the right order of magnitude for rectified diffusion growth rates so a closer examination of the problem was made.

Figure 11 shows computer integration curves of the time required to grow from a range of initial sizes to resonance size for various values of the acoustic intensity. An interesting aspect of the curves is a leveling off of the times to a maximum value for initial radii less than about 0.5μm. This asymptotic behavior is of general interest, and can be demonstrated by studying the differential equation directly. Equation 16 is a complicated equation near resonance but if it is examined far enough away from resonance, it can be integrated directly. If it is assumed that $\beta^2 << 1$, then Eq. 16 can be written as

Figure 10a. Oscilloscope trace of subharmonic emissions from an insonated root tip. The sweep rate was 0.5 ms/cm and the acoustic intensity was about 30 W/cm^2.

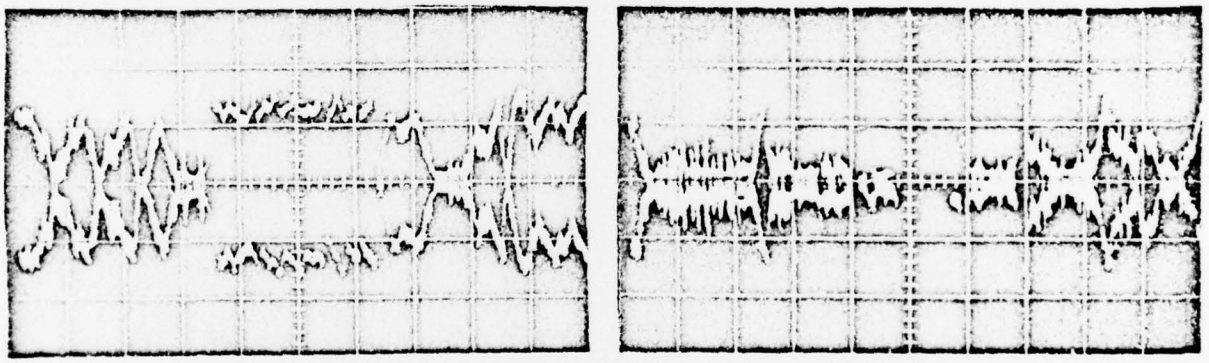

Figures 10b & 10c. Oscilloscope trace of subharmonic emissions from an insonated root tip. The sweep rate was 0.5 ms/cm and the acoustic intensity was about 30 W/cm^2. Figure b was taken immediately after the onset of subharmonic emission; Figure c was taken approximately 100 seconds later.

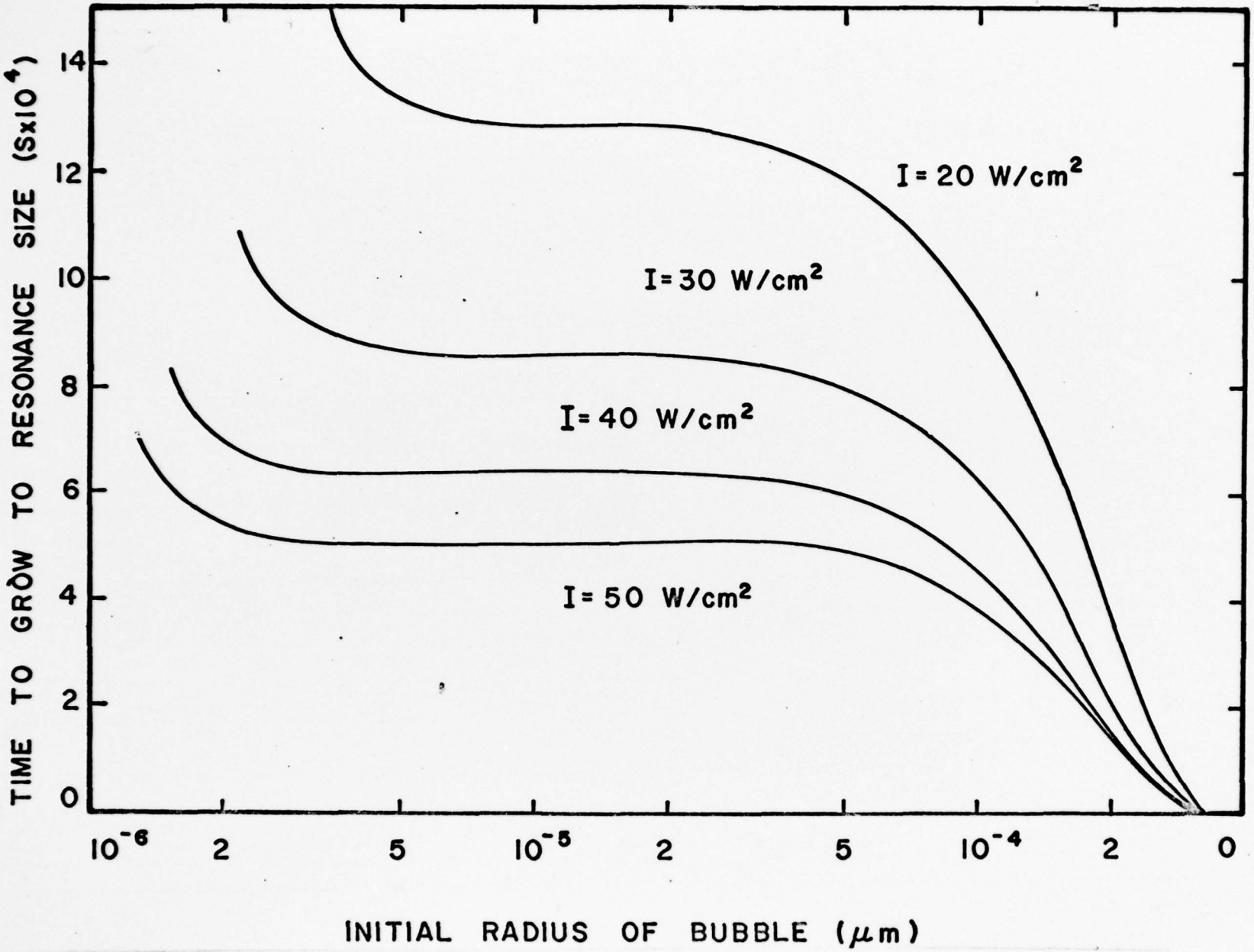

Figure 11. Growth times required to grow from an initial size to resonance size for various values of the acoustic intensity. Curves are for free bubbles in saturated water.

$$\frac{dR}{dt} = \frac{Dd}{R}\left(\frac{2}{3}\left(\frac{P_A}{P_0}\right)^2\right) - \frac{2\sigma Dd}{P_0 R^2} \quad . \tag{17}$$

If the substitutions $A = \frac{2}{3}\left(\frac{P_A}{P_0}\right)^2 \frac{Dd}{}$, and $B = \frac{2\sigma Dd}{P_0}$ are made, then this equation can be written as

$$\int_{T_0}^{T} dt = \int_{R_0}^{R} \frac{R^2 dR}{AR-B} \, , \tag{18}$$

which can be integrated by parts to give an estimate of the time Δt required to grow from an initial radius R_0 to a final radius R (that is significantly less than R_{res}) to be

$$\Delta t = \frac{B}{A^2}\left[\frac{A}{2B}(R-R_0)^2 + (R-R_0) + \frac{B}{A}\ell n\left(\frac{B-AR_0}{B-AR}\right)\right] \quad . \tag{19}$$

This equation shows two interesting aspects. First, for certain values of the initial radius, viz., $R_t \leq B/A$, an infinite time is required for growth. But $R_t = B/A$ implies that $\frac{2}{3}\left(\frac{P_A}{P_0}\right)^2 = \frac{2\sigma}{P_0 R_t}$ and this is essentially the threshold for rectified diffusion. For intensities lower than the threshold value, the bubble will dissolve. For our lowest intensity of interest, I = 20 W/cm^2, $R_t = 3.5 \times 10^{-6}$ cm. Note that slightly above this value the second and third terms in the equation are relatively unimportant due to the small value of B/A ($\sim 10^{-6}$) and the time is essentially governed by the simple relationship

$$\Delta t = \frac{(R-R_0)^2}{2A} = \frac{3R_0^2}{4Dd}\left(\frac{P_0}{P_A}\right)^2 (1 - R/R_0)^2 \quad . \tag{20}$$

Thus, the asymptotic approach of Δt to a constant value for low R is easily shown and is given by

$$\Delta t = \frac{3R_0^2}{4Dd} \left(\frac{P_0}{P_A}\right)^2 , \tag{21}$$

with the caveat that $R > 3\sigma P_0/P_A^2$. This result asserts that a relatively large range of bubble sizes will grow to resonance size in the same time interval, an interesting and important deduction.

It is also of interest to examine the behavior of air bubbles that may be larger than resonance size. Consequently, Eq. 16 was numerically integrated to show the time required for a bubble to grow from an initial radius to its maximum size. Figure 12 shows the growth of a bubble with initial size $R = 5.0 \times 10^{-6}$. Note that the bubble grows progressively more rapidly as it approaches resonance but then grows steadily until it approaches asymptotically a maximum size. If Eq. 16 is examined directly, it is seen that if the surface tension term is neglected, then the growth rate becomes zero for $\beta^2 = 8$, and negative for larger values of β^2. Since $\beta^2 = 1$ is the resonance condition, it is seen that air bubbles with radii larger than $\sqrt{8}$ times their resonance size will actually be forced to smaller sizes by rectified diffusion.

In Fig. 10b and c are two oscilloscope traces of the emitted subharmonic output from an insonated root tip. The first trace was taken immediately after the acoustic emission commenced; the second was taken nearly 100 seconds later. The first trace shows a few relatively long and relatively consistent growth times; the second shows several relatively

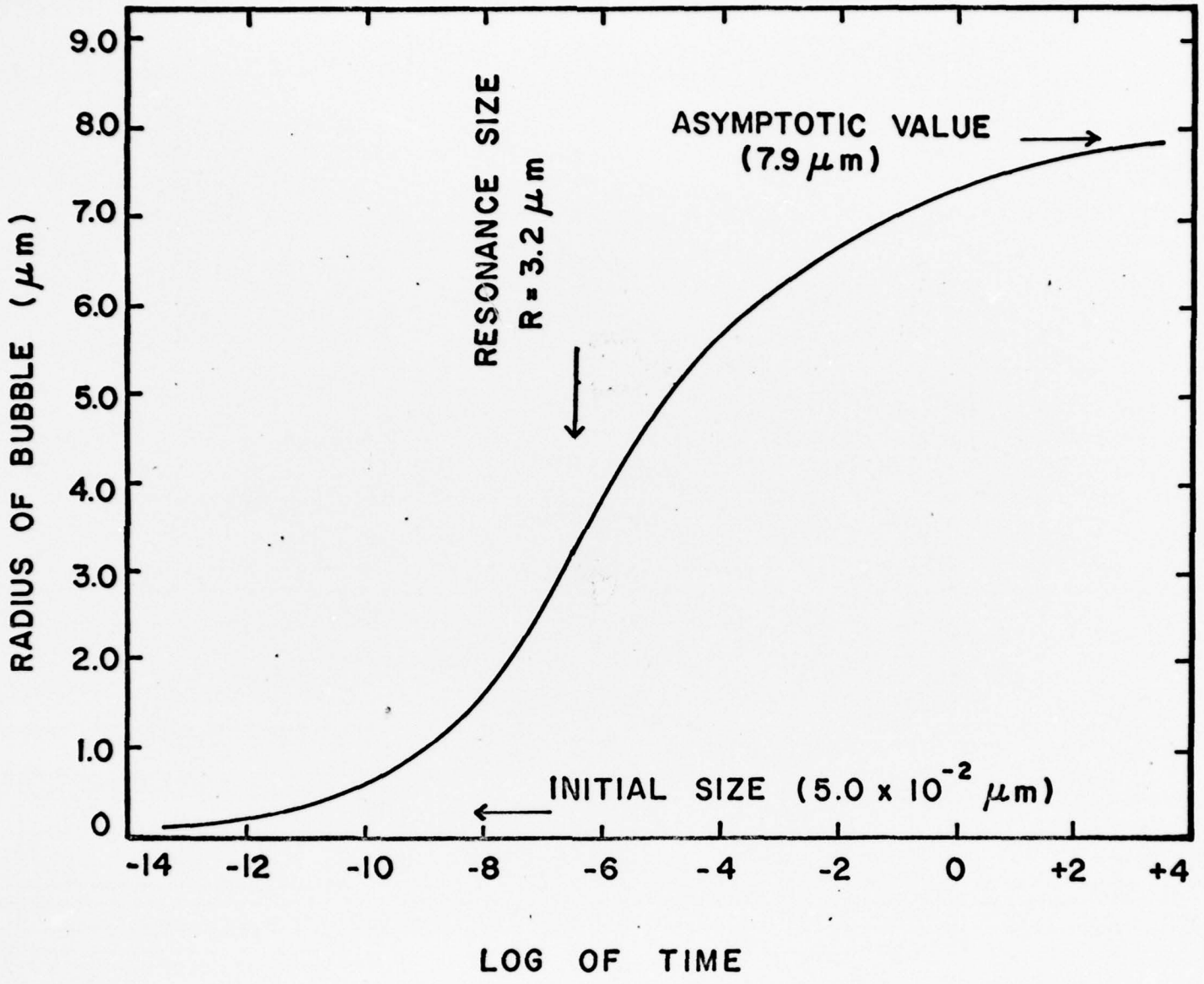

Figure 12. Life history of growth of bubble. This is for an intensity of 30 W/cm^2 and a frequency of 1 MHz.

short and relatively inconsistent growth times. These traces suggest, in the light of the above theoretical analysis, that air bubbles may be growing to resonance size from nuclei, and then breaking up into a group of smaller bubbles by surface wave activity.

DISCUSSION

The analysis of acoustic emissions from insonated root tips indicated that it is unlikely that the relatively long delay time of seconds between the commencement of the irradiation and the onset of subharmonic and white noise is due to growth of air bubbles by rectified diffusion. Theoretical examination of growth from a range of nuclei sizes indicates growth times on the order of tenths of milliseconds. It is possible that certain constraints may exist within the root system that would slow down rectified diffusion but none seem likely to affect it to four orders of magnitude. Further, since oscilloscope scans of the subharmonic emissions show growth times of the radiated signal on the order of 0.3 ms, and since calculated growth times for rectified diffusion are in the range 0 to 1.3 ms, it seems likely that air bubbles are growing by rectified diffusion but at the shorter times rather than the longer. Unstable growth of cavities through vaporous cavitation can occur in these growth times also and must be considered as an alternative explanation. Its examination is too complicated to consider here however.

There is a mechanism that will lead to delay times on the order of 10 seconds and to subsequent violent activity. The time required for

air bubbles much larger than resonance size to reduce in size, is on the order of seconds. For example, for an intensity of 30 W/cm, three seconds is required for an air bubble of 10μ radius to reduce to a radius of 7.9μm, the radius for which rectified diffusion ceases at a frequency of 1 MHz; the time required for the radius to change from 20μm to 8.3μm is 17 sec. Measurements of the intercellular spaces are on this order of magnitude.[16] Thus, it is possible that this intercellular gas is reduced in size until it can develop surface waves. These surface waves cause the bubble to break up into several small bubbles, which grow by rectified diffusion to resonance size again and again.

ACKNOWLEDGEMENT

The author wishes to acknowledge the use of the oscilloscope traces and acoustic emission data obtained by J. Morris and W. T. Coakley as well as their many helpful suggestions and comments.

LIST OF REFERENCES

1. E. N. Harvey, D. K. Barnes, W. D. McElrory, A. H. Whitely, D. C. Pease and K. W. Cooper, J. Cell. Comp. Physiol. 24, 1 (1944).

2. J. E. Barger, "Thresholds of Acoustic Cavitation," Tech. Memo. No. 57, Acoust. Res. Lab., Harvard Univ., 1964.

3. M. Strasberg, J. Acoust. Soc. Amer. 31, 163-176 (1959).

4. R. E. Apfel, J. Acoust. Soc. Amer. 48, 1179 (1970).

5. J. W. Holl, J. Basic Engr. Trans. ASME, D, Vol. 92, 681 (1970).

6. R. E. Apfel, "Vapor Cavity Formation in Liquids," Tech. Memo. No. 62, Acoust. Res. Lab., Harvard Univ., 1970.

7. A. T. Ellis, J. G. Waugh and R. Y. Ting, J. Basic Engr. Trans. ASME, D, Vol. 92, 459 (1970).

8. J. W. Hoyt, J. Fluids Engr. Trans. ASME, I, Vol. 98, 106 (1976).

9. A. T. Ellis, Comments on paper by J. W. Hoyt, J. Fluids Engr. Trans. ASME, I, Vol. 98, 106 (1976).

10. A. W. Adamson, Physical Chemistry of Surfaces (Interscience Pub. Inc., New York, 1967) pp. 113-139.

11. C. G. L. Furmidge, J. Colloid. Sci. 17, 309-324 (1962).

12. D. Bargeman and F. Van Voorst Vader, J. Colloid. Sci. 42, 467-472 (1973).

13. W. Lanterborn, private communication.

14. W. I. Galloway, J. Acoust. Soc. Amer. 26, 849 (1954).

15. F. L. Cataldo, M. W. Miller and G. E. Kaufman, Env. and Exp. Bot. 16, 89-91 (1976).

16. B. I. Bleaney and R. Oliver, Brit. J. Radiol. 45, 358-361 (1972).

17. W. D. Gregory, M. W. Miller, E. L. Carstensen, F. Cataldo, and M. M. Ready, Brit. J. Radiol. 47, 122-129 (1974).

18. A. Gershoy, D. L. Miller and W. L. Nyborg. Ultrasound in Medicine, Vol. 2, D. N. White and R. Barnes, Eds. (Plenum Press, New York, 1976) pp. 501-511.

19. W. T. Coakley and J. Morris, Conf. on Acoustic Cavitation, Bournemouth, U.K., 1977 (to be published in proc. of Inst. of Acoustics).

20. A. I. Eller, J. Acoust. Soc. Amer. 52, 1447-1449 (1972).

21. L. A. Crum and A. I. Eller, "The Motion of Bubbles in a Stationary Sound Field," Tech. Memo. No. 61, Acoust. Res. Lab., Harvard Univ. (1969).

June 1978

REPORTS DISTRIBUTION LIST FOR ONR PHYSICS PROGRAM OFFICE
UNCLASSIFIED CONTRACTS

Director
Defense Advanced Research Projects Agency
Attn: Technical Library
1400 Wilson Blvd.
Arlington, Virginia 22209
3 copies

Office of Naval Research
Physics Program Office (Code 421)
800 North Quincy Street
Arlington, Virginia 22217
3 copies

Office of Naval Research
Assistant Chief for Technology (Code 200)
800 No. th Quincy Street
Arlington, Virginia 22217
1 copy

Naval Research Laboratory
Department of the Navy
Attn: Technical Library
Washington, D. C. 20375
3 copies

Office of the Director of Defense
Research and Engineering
Information Office Library Branch
The Pentagon
Washington, D. C. 20301
3 copies

U. S. Army Research Office
Box 12211
Research Triangle Park
North Carolina 27709
2 copies

Defense Documentation Center
Cameron Station (TC)
Alexandria, Virginia 22314
12 copies

Director, National Bureau of Standards
Attn: Technical Library
Washington, DC 20234
1 copy

Commanding Officer
Office of Naval Research Branch Office
536 South Clark Street
Chicago, Illinois 60605
3 copies

Commanding Officer — 3 copies
Office of Naval Research Branch Office
1030 East Green Street
Pasadena, California 91101

San Francisco Area Office — 3 copies
Office of Naval Research
One Hallidie Plaza
Suite 601
San Francisco, California 94102

Commanding Officer — 3 copies
Office of Naval Research Branch Office
666 Summer Street
Boston, Massachusetts 02210

New York Area Office — 1 copy
Office of Naval Research
715 Broadway, 5th Floor
New York, New York 10003

Director — 1 copy
U. S. Army Engineering Research
and Development Laboratories
Attn: Technical Documents Center
Fort Belvoir, Virginia 22060

ODDR&E Advisory Group on Electron Devices — 3 copies
201 Varick Street
New York, New York 10014

Air Force Office of Scientific Research — 1 copy
Department of the Air Force
Bolling AFB, D. C. 22209

Air Force Weapons Laboratory — 1 copy
Technical Library
Kirtland Air Force Base
Albuquerque, New Mexico 87117

Air Force Avionics Laboratory — 1 copy
Air Force Systems Command
Technical Library
Wright-Patterson Air Force Base
Dayton, Ohio 45433

Lawrence Livermore Laboratory — 1 copy
Attn: Dr. W. F. Krupke
University of California
P. O. Box 808
Livermore, California 94550

Harry Diamond Laboratories — 1 copy
Technical Library
2800 Powder Mill Road
Adelphi, Maryland 20783

Naval Air Development Center — 1 copy
Attn: Technical Library
Johnsville
Warminster, Pennsylvania 18974

Naval Weapons Center — 1 copy
Technical Library (Code 753)
China Lake, California 93555

Naval Training Equipment Center — 1 copy
Technical Library
Orlando, Florida 32813

Naval Underwater Systems Center — 1 copy
Technical Library
New London, Connecticut 06320

Commandant of the Marine Corps — 1 copy
Scientific Advisor (Code RD-1)
Washington, DC 20380

Naval Ordnance Station — 1 copy
Technical Library
Indian Head, Maryland 20640

Naval Postgraduate School — 1 copy
Technical Library (Code 0212)
Monterey, California 93940

Naval Missile Center — 1 copy
Technical Library (Code 5632.2)
Point Mugu, California 93010

Naval Ordnance Station — 1 copy
Technical Library
Louisville, Kentucky 40214

Commanding Officer — 1 copy
Naval Ocean Research & Development Activity
Technical Library
NSTL Station, Mississippi 39529

Naval Explosive Ordnance Disposal Facility — 1 copy
Technical Library
Indian Head, Maryland 20640

Naval Ocean Systems Center — 1 copy
Technical Library
San Diego, California 92152

Naval Surface Weapons Center — 1 copy
Technical Library
Dahlgren, Virginia 22448

Naval Surface Weapons Center (White Oak) — 1 copy
Technical Library
Silver Spring, Maryland 20910

Naval Ship Research and Development Center — 1 copy
Central Library (Code L42 and L43)
Bethesda, Maryland 20084

Naval Avionics Facility — 1 copy
Technical Library
Indianapolis, Indiana 46218